Next-to-leading order corrections to light-quark mixed QCD-EW contributions to Higgs boson production

Matteo Becchetti[*]

Dipartimento di Fisica, Università di Torino and INFN Sezione di Torino,
Via Pietro Giuria 1, I-10125 Torino, Italy

Roberto Bonciani[†]

Dipartimento di Fisica, Università di Roma "La Sapienza" and INFN Sezione di Roma,
Piazzale Aldo Moro 2, 00185 Roma, Italy

Vittorio Del Duca[‡]

ETH Zürich, Institut für theoretische Physik, Wolfgang-Pauli Straße 27, 8093, Zürich, Switzerland
and INFN, Laboratori Nazionali di Frascati, 00044 Frascati (RM), Italy

Valentin Hirschi,[§] Francesco Moriello,[‖] and Armin Schweitzer[¶]

ETH Zürich, Institut für theoretische Physik, Wolfgang-Pauli Straße 27, 8093 Zürich, Switzerland

We present for the first time the exact next-to-leading-order QCD corrections to the light-quark part of the mixed QCD-EW contributions to Higgs production via gluon fusion at the Large Hadron Collider, for a center-of-mass energy of 13 TeV, with exact EW-boson mass dependence. The relevant two-loop real-emission matrix element is computed using a dynamic one-dimensional series expansion strategy whose stability and speed allows for a numerical phase-space integration using local IR subtraction counterterms. For the choice of renormalization (μ_R) and factorization (μ_F) scales, $\mu_R = \mu_F = M_H$, we find $\sigma_{gg \to H+X}^{(\alpha_s^2 \alpha^2 + \alpha_s^3 \alpha^2)} = 1.467(2)_{-14.6\%}^{+18.7\%}(\mu_R \text{ var}) \pm 2\% \,(\text{PDF})$ pb, which we use to provide the best result, including an estimate of suppressed contributions: $\sigma_{pp \to H+X}^{(\text{EW,best})} = 2.11 \pm 0.28 \,(\text{theory})$ pb.

I. INTRODUCTION

After the discovery of the Higgs boson with the Large Hadron Collider (LHC) at CERN in 2012 [1,2], the work of the LHC community has focused on the study of the Higgs sector, which provides a stringent test of the Standard Model of particles (SM) and a fertile environment for the search of new physics (NP) signals [3–15].

A key ingredient for predictions of Higgs observables is accurate knowledge of the Higgs production cross section in gluon fusion, which at the LHC is by far the dominant production mode. The coupling of the Higgs boson to gluons is mediated by a heavy-quark loop. The Higgs production cross section was computed at leading order in the 1970s [16], and at next-to-leading order (NLO) in the strong coupling constant α_s in the 1990s [17,18]. NLO QCD corrections are sizable ($\sim 80\%$–100%), undermining the reliability of the perturbative expansion in α_s of the production cross section. The next-to-next-to-leading-order (NNLO) [19–21] and the next-to-next-to-next-to-leading-order (N^3LO) [22,23] corrections in α_s have been computed in the Higgs effective field theory (HEFT) approach—i.e., in the limit of a top quark much heavier than the Higgs boson, $M_T \gg M_H$, with all other quarks taken as massless, which replaces the loop-mediated coupling with an effective tree-level coupling. The NNLO corrections turn out to be significant ($\sim 10\%$–20%), but with a reduced scale-dependent uncertainty. The N^3LO corrections turn out to be small ($\sim 4\%$–6%) [24], with a renormalization/factorization scale variation of less than 2%.

The high accuracy of the N^3LO corrections calls for the evaluation of finite quark-mass effects and electroweak

[*]matteo.becchetti@unito.it
[†]roberto.bonciani@roma1.infn.it
[‡]delducav@itp.phys.ethz.ch
[§]valentin.hirschi@gmail.com
[‖]fmoriell@itp.phys.ethz.ch
[¶]armin.schweitzer@phys.ethz.ch

contributions. Finite quark-mass effects are known through
NLO [18,25–30] and contribute a $\sim -7\%$ change [29] to
the cross section. Although the relevant ingredients—
double-virtual [31–33], real-virtual [34–36], and double-
real [37,38]—of the computation of the finite quark-mass
effects at NNLO are available, such a computation has not
been performed yet. At NNLO, top-quark mass effects have
been estimated through a power expansion in M_H/M_T
[39–41] and found to be $\sim 1\%$. Light-quark mass effects—
in particular, the top-bottom interference—are not yet
known at NNLO.

   Mixed QCD-electroweak (EW) effects arise at two
loops[1]—i.e., at $\mathcal{O}(\alpha^2\alpha_s^2)$. They are due to the gluons
coupling to EW bosons $V = W$, Z through a quark loop,
followed by the gauge coupling of the EW bosons to the
Higgs boson. Mixed QCD-EW contributions were calcu-
lated for the light-quark loop [42–44], for the heavy-quark
loop [45], and with full quark-mass dependence [45], and
were found to increase the N³LO cross section by about 2%
[24]. Since this increase is of the order of the residual QCD
uncertainty, it is important to compute the NLO corrections
in α_s. Because the largest part ($\sim$98% [44]) of the increase
at $\mathcal{O}(\alpha^2\alpha_s^2)$ is due to the light-quark part of the mixed QCD-
EW contributions, the evaluation of the NLO corrections
has been aimed at the light-quark part. These corrections
were evaluated in the limit where the Higgs mass is much
smaller than the EW boson masses, $M_H \ll M_V$ [46], and
they turned out to be sizable.

   The $\mathcal{O}(\alpha^2\alpha_s^3)$ corrections consist of three parts: the one-
loop $2 \to 3$, the three-loop $2 \to 1$, and the two-loop $2 \to 2$,
with sample diagrams shown in the first column of Fig. 1.
In Ref. [47], the one-loop $2 \to 3$ processes were computed
and found to yield a negligible contribution. The three-loop
contribution was evaluated analytically and expressed in
terms of multiple polylogarithms (MPLs) [48]. In Ref. [49],
the soft part of the two-loop $2 \to 2$ process was added. In
Ref. [50], the total cross section was evaluated in the small
EW-boson mass limit, $M_V \ll M_H$. The planar master
integrals (MIs) for the two-loop $gg \to Hg$ process with
the exact EW-boson mass were published in Ref. [51] and
recently, in Ref. [52], the complete helicity amplitudes,
including the nonplanar diagrams, were presented. The
calculation was done analytically, expressing the results in
terms of MPLs.

   In this work, we perform an independent computation of
the amplitude and of the MIs, which are evaluated by using
the series solution method of Ref. [53], and we present the
NLO QCD corrections to the total cross section for Higgs
production via gluon fusion at the LHC, due to the light-
quark part of the mixed QCD-EW contributions, with exact
EW boson mass dependence.

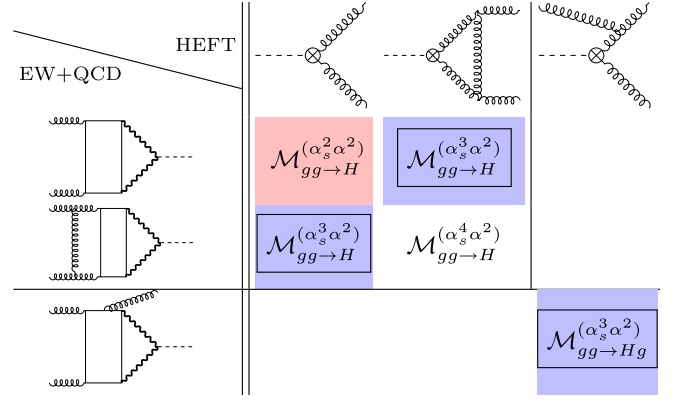[1]We count all factorized coupling constants except the strong
coupling as α.

FIG. 1.   Overview of the relevant interferences necessary for the
computation of the hadronic cross section $\sigma_{gg\to H+X}^{(\alpha_s^2\alpha^2+\alpha_s^3\alpha^2)}$. The red
cell is the LO, and cells highlighted in blue are part of the NLO
contribution. Amplitudes are denoted by a single representative
diagram. Curly lines denote gluons, wavy lines are massive weak
gauge bosons, continuous straight lines are massless quarks, and
the dashed line represents the Higgs boson.

II. CALCULATION

A. Loop amplitudes

   The computation of the two-loop $gg \to Hg$ amplitude for
the matrix element $\mathcal{M}_{gg\to Hg}^{(\alpha_s^3\alpha^2)}$ (see Fig. 1) is performed by
using the series expansion method of Ref. [53].
Specifically, we reduce the amplitude to MIs by using
computer programs [54–56] for the solution of integration-
by-parts identities (IBPs) [57–59] and Lorentz-invariance
identities (LI) [60]. By taking advantage of these identities,
we define a system of differential equations [61–64] for a
basis of canonical MIs [65]. The canonical basis is found by
using the methods of Refs. [65–71], and the corresponding
differential equations are solved in terms of generalized
power series, as described in Ref. [53]. The system of
differential equations uniquely defines the solution when
imposing boundary conditions at a special kinematic point.
We consider the infinite EW boson mass limit as our initial
boundary point. The numerical evaluation of the relevant
scattering amplitudes by means of the generalized power
series approach is well suited for Monte Carlo phase-space
integrations. Moreover, the analytic continuation of the
generalized power series to the physical regions is fully
algorithmic.

   The series solution strategy can be summarized as
follows: We transport the integrals from a known boundary
point to a phase-space point of interest by solving the
differential equations in terms of generalized power series
along the line connecting the pair of points. This is done
dynamically for every new phase-space point. When the
line crosses a physical threshold, the analytic continuation
is defined by assigning a vanishing imaginary part to the
line parameter, in accordance with Feynman prescription.
By construction, the nonanalytic terms of the series are

logarithms and rational powers of the line parameter, and their analytic continuation is elementary. In order to improve the efficiency of the evaluations, we consider a precomputed grid of about 5000 physical phase-space boundary points. In this way, the series solution can be found along lines connecting pairs of points separated by a relatively short distance. In general, these lines cross fewer singular points of the differential equations, and they require, for fixed precision, a lower truncation order of the series, considerably reducing the average evaluation time. In this work, we consider truncated power series which guarantee a precision for the numerical evaluations of the integral basis of at least 16 digits after the decimal point. The average time for one form-factor evaluation on one CPU core is $\mathcal{O}(1 \text{ min})$, ranging from $\mathcal{O}(30 \text{ sec})$ up to $\mathcal{O}(10 \text{ min})$ for input kinematic configurations featuring large-scale hierarchies.

We verify our computation against Ref. [52] and report benchmark values for the relevant matrix elements in the Appendix. As for the three- and two-loop matrix elements of the $gg \to H$ process [$\mathcal{M}_{gg \to H}^{(\alpha_s^3 \alpha^2)}$ and $\mathcal{M}_{gg \to H}^{(\alpha_s^2 \alpha^2)}$, respectively, in Fig. 1], we use the results presented in Refs. [48,72].

B. Phase-space integration and infrared regularization

Infrared (IR) divergences are locally subtracted using two different paradigms for cross-validation: first, the Frixione, Kunszt, and Signer (FKS) subtraction scheme [73] and second, a modified version [74,75] of the COLORFUL [76,77] scheme at NLO. To the best of our knowledge, this is the first time that a two-loop matrix element with implicit phase-space IR divergences has been numerically integrated using local subtraction counterterms. To achieve this, we encoded the loop amplitudes discussed in the previous paragraph as form factors of effective vertices in the Universal FeynRules Output (UFO) [78] model. We then created a custom plugin made publicly available[2] for the MadGraph5_aMC@NLO program [79], allowing for the generation of a standalone library for the evaluation of all matrix elements entering our computation. We finally customized the generation output of MadGraph5_aMC@NLO for the NLO QCD correction of inclusive Higgs hadroproduction within the Higgs Effective Theory (HEFT) in order to accommodate the aforementioned matrix elements as well as an offline parallelization pipeline.

We validated our results against those obtained using a modified version of the NLO implementation [77] of the COLORFUL subtraction scheme rendered suitable for the computation of a Higgs-inclusive cross section and implemented in the private extension of MadGraph5_aMC@NLO already featured in Ref. [47]. In that variant, the local soft
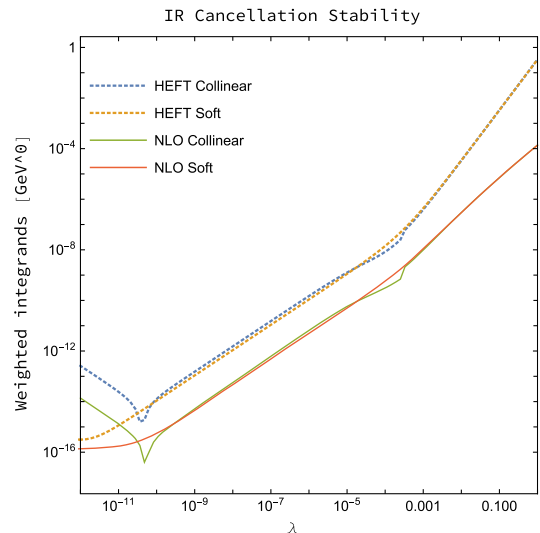

FIG. 2. Numerical stability of the two-loop real-emission matrix element, locally subtracted with our modified implementation of COLORFUL, compared to their HEFT tree-level counterpart when approaching the soft and collinear limits. The approach parameter λ is defined so that the scaling of the real-emission matrix when approaching the IR limit is λ^{-1}. The weighted integrand shown includes the Jacobian of the parametrization so that it must scale like λ^α with $\alpha > \frac{1}{2}$ in order to be integrable.

counterterm uses a mapping recoiling against initial states (see Ref. [75] and Sec. 5.3.3 of Ref. [74]) and *locally* identically cancels against its soft-collinear counterpart. This is a consequence of the fact that our real-emission matrix element only features soft emission from an initial-initial dipole. The initial-final collinear counterterms alone are thus sufficient to regularize the infrared (IR) divergences involved in our computation. We showcase the stability of the real-emission matrix element in Fig. 2 by investigating the quality of its cancellation against local IR counterterms both in the collinear and soft limits. We find stability on par with that obtained in HEFT when considering tree-level real-emission matrix elements, where the limiting factor is the double-precision accuracy of the input kinematics. We also tested the independence of our result on the arbitrary cutoff of the local IR collinear counterterms (parameter y'_0 in Ref. [77]). We verified that our two independent implementations of the FKS and COLORFUL IR subtraction procedure give consistent results.

III. RESULTS

We carry out our computation in the Standard Model (SM) using the relevant input parameters given in Table I, where the masses of the gauge bosons are chosen in order to align with the literature [48,72], and the weak coupling follows from the gauge relation with G_F. The Weinberg mixing angle is determined by $\cos\theta_W = M_W/M_Z$.

---

[2] https://bitbucket.org/aschweitzer/mg5_higgs_ew_plugin/ or http://madgraph.physics.illinois.edu/Downloads/PLUGIN/higgsew.tar.gz.

TABLE I.   Standard Model parameters used for obtaining all numerical results presented in this work. Dimensionful parameters are given in GeV unless indicated otherwise. All particle widths are set to zero.

Parameter	Value	Parameter	Value
PDF set	PDF4LHC15_nlo_30	$\mu_R = \mu_F$	M_H
$\alpha_S(\mu_R)$	As per PDF set.	G_F	$\frac{\pi\alpha}{\sqrt{2}M_W^2(1-M_W^2/M_Z^2)}$
$\sqrt{\hat{s}}$	13 TeV	α^{-1}	132.507
M_Z	91.1876	V_{ij}^{CKM}	δ_{ij}
M_W	80.3845	M_H	125.09

We remind the reader that we consider for the W-exchange only the first two light-quark generations, whereas the Z-exchange also receives contributions from massless b quarks, as discussed in Refs. [48,72]. We furthermore neglect the contribution from $gg \to Hq\bar{q}$ (computed to be below 0.1 pb in Ref. [47]).

For comparison purposes, we start by providing here the cross section for the hadroproduction of a Higgs boson, computed at LO and NLO QCD in HEFT:

$$\sigma_{gg \to H+X}^{(\text{HEFT},\alpha_s^2\alpha)} = 13.209_{-17.3\%-2.0\%}^{+23.4\%+2.0\%} \text{ pb}, \qquad (1)$$

$$\sigma_{gg \to H+X}^{(\text{HEFT},\alpha_s^2\alpha+\alpha_s^3\alpha)} = 30.484_{-15.3\%-1.9\%}^{+19.8\%+1.9\%} \text{ pb}, \qquad (2)$$

where the first set of uncertainties corresponds to the $(\frac{1}{2}, 1, 2)$ μ_R scale variation. The second set reports the PDF uncertainty obtained within MadGraph5_aMC@NLO, which uses the LHAPDF [80] interface. At this point, the factorization scale variation is insofar not a reliable error estimate, since we only consider initial-state gluons, and its size will therefore depend strongly on the chosen central scale. However, the reduction of the scale dependence can be seen in Eq. (20), which also includes an estimate for the qg channel. Our result for the correction from light quarks to the mixed QCD-EW contribution to the inclusive Higgs production cross section is

$$\sigma_{gg \to H+X}^{(\alpha_s^2\alpha^2)} = 0.68739_{-17.3\%-2.0\%}^{+23.4\%+2.0\%} \text{ pb}, \qquad (3)$$

$$\sigma_{gg \to H+X}^{(\alpha_s^2\alpha^2+\alpha_s^3\alpha^2)} = 1.467(2)_{-14.6\%-2.0\%}^{+18.7\%+2.0\%} \text{ pb}. \qquad (4)$$

The resulting pure NLO QCD correction of order $\mathcal{O}(\alpha_s^3\alpha^2)$ is 0.780(2) pb and was obtained from 50 000 evaluations of the real-emission matrix element in our private implementation of the COLORFUL NLO subtraction scheme. The gluon-initiated cross section with exact EW-boson mass dependence in the virtual contributions and the real contribution treated in the soft-gluon, the massless, and the infinite mass approximations increase the pure gluon-induced HEFT NLO cross section by 5.4% [49], 5.4% [50], and 5.2% [50], respectively, whereas our exact
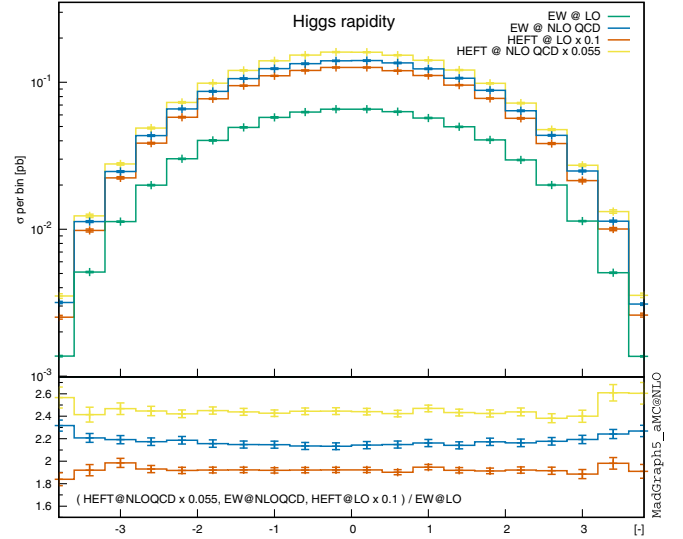

FIG. 3.   Differential prediction for the $\mathcal{O}(\alpha_s^3\alpha^2)$ correction to the Higgs rapidity distribution.

computation, with $\mu_R = \mu_F = \frac{1}{2}M_H$ and $\alpha^{-1} = 128.0$ as in Refs. [49,50] yields 5.1%. Our result therefore lies within the original uncertainty assigned to the factorization estimate of 5% ± 1% given in Ref. [20] and used in Ref. [24]. We furthermore notice the small reduction of the scale uncertainty when including NLO corrections. This slow convergence is a known feature of gluon-fusion Higgs production.

We present the two most relevant differential predictions in Figs. 3 and 4. First, in Fig. 3, we show the NLO-accurate Higgs rapidity distribution, which reveals the expected flat differential K factor, both for the EW effects with respect to the HEFT approximation and for the QCD corrections. Second, in Fig. 4, we show the Higgs transverse momentum distribution, which is accurate at leading order, and which we compare to its HEFT counterpart whose spectrum is harder. We stress that Fig. 4 has no direct phenomenological relevance, given that quark mass effects are poised to affect the shape of the Higgs transverse momentum distributions [81]. Even though we provide an estimate of these mass effects on the fully inclusive level, to obtain the correct high p_T-tail of the distribution, the quark mass effects in the EW amplitudes would also need to be considered. These amplitudes are beyond the current state of the art in multiloop computations.

We also report in Fig. 5 on the shape of the kinematic dependence of $\mathcal{M}_{gg \to Hg}^{(\alpha_s^3\alpha^2)}$ relative to that of $\mathcal{M}_{gg \to Hg}^{(\alpha_s^3\alpha)}$. We find that the dependence of this ratio on z is more marked. In particular, we see that the ratio stabilizes rapidly as we approach the production threshold $z \to 1$, which amounts to the bulk of the relevant phase space. This is in line with the observation that factorization-like approximations provide a good approximation of the total cross section. For $l \sim 0.5$, the limit $z \to 0$ corresponds to larger values of the Higgs transverse momentum, where we see that the
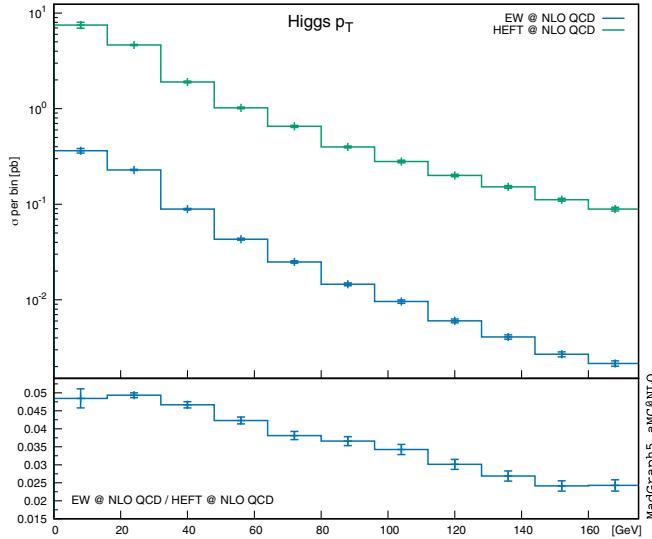
FIG. 4. Differential prediction for the $\mathcal{O}(\alpha_s^3\alpha^2)$ EW contribution to the Higgs transverse momentum distribution, compared to its LO HEFT counterpart.

two-loop EW matrix element is of smaller magnitude than that of its tree-level HEFT counterpart, as anticipated from the transverse momentum distribution shown in Fig. 4.

The *factorization hypothesis* of the Higgs cross section is

$$\sigma_{gg\to H+X}^{(\sum_i \alpha_s^{i+2}(\alpha+\alpha^2))} = C^2(\tilde{\sigma}_{gg\to H+X}^{(\alpha_s^2\alpha)} + \tilde{\sigma}_{gg\to H+X}^{(\alpha_s^3\alpha)} + \cdots), \quad (5)$$

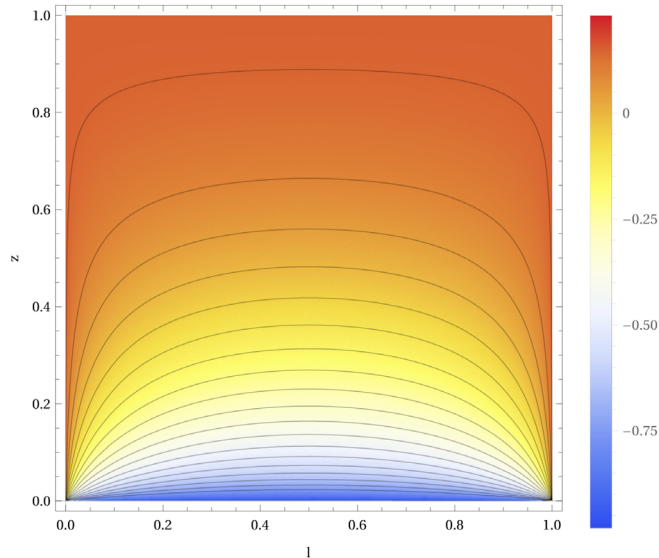FIG. 5. Plot of the quantity $\frac{(\mathcal{M}_{gg\to Hg}^{(\alpha_s^3\alpha^2)}/\mathcal{M}_{gg\to Hg}^{(\alpha_s^3\alpha)} - R^{NLO})}{R^{NLO}}$ with $R^{NLO} = \sigma_{gg\to H+X}^{(\alpha_s^3\alpha^2)}/\sigma_{gg\to H+X}^{(HEFT,\alpha_s^3\alpha)}$, in terms of the rescaled kinematic invariants $z = M_H^2/s$ and $l = t/(M_H^2 - s)$, for a sample of $\sim$150 000 phase-space points. The lines of constant deviation span the range $[-0.75, 0.15]$ in increments of 0.05.

with

$$C = \sum_{i=0} \left(\frac{\alpha_s}{\pi}\right)^i (C_{QCD}^{(i)} + \lambda_{EW} C_w^{(i)}) \quad (6)$$

and $C_w^{(0)} = C_{QCD}^{(0)} = 1$, $C_{QCD}^{(1)} = 11/4$. In terms of our quantities from Eqs. (1)–(4), we have

$$\tilde{\sigma}_{gg\to H+X}^{(\alpha_s^2\alpha)} = \sigma_{gg\to H+X}^{(HEFT,\alpha_s^2\alpha)}, \quad (7)$$

$$\tilde{\sigma}_{gg\to H+X}^{(\alpha_s^3\alpha)} = -2C_{QCD}^{(1)}\sigma_{gg\to H+X}^{(HEFT,\alpha_s^2\alpha)} + \sigma_{gg\to H+X}^{(HEFT,\alpha_s^3\alpha)}, \quad (8)$$

$$\lambda_{EW} = \frac{\sigma_{gg\to H+X}^{(\alpha_s^2\alpha^2)}}{2\sigma_{gg\to H+X}^{(HEFT,\alpha_s^2\alpha)}}, \quad (9)$$

$$C_w^{(1)} = C_{QCD}^{(1)} + \left(\frac{\alpha_s}{\pi}\right)^{-1}\left(\frac{\sigma_{gg\to H+X}^{(\alpha_s^3\alpha^2)}}{\sigma_{gg\to H+X}^{(\alpha_s^2\alpha^2)}} - \frac{\sigma_{gg\to H+X}^{(HEFT,\alpha_s^3\alpha)}}{\sigma_{gg\to H+X}^{(HEFT,\alpha_s^2\alpha)}}\right). \quad (10)$$

For $\mu_R = \mu_F$, our exact computation thus yields

$$\lambda_{EW} = 0.026, \quad (11)$$

$$C_w^{(1)}|_{\mu_R=\frac{1}{2}M_H} = -1.700, \qquad C_w^{(1)}|_{\mu_R=M_H} = -2.072, \quad (12)$$

which is quite different from $C_w^{(1)} = 7/6$ as estimated in the infinite boson-mass approximation; however, it is still within the uncertainty estimate of Ref. [24].

Remaining corrections to our computation: We identify three main contributions still unaccounted for in our computation of the mixed QCD-EW cross section. We provide here an estimate for each, together with an associated uncertainty:

(1) *Heavy-quark (mass) effects* in the QCD amplitudes can be estimated by using

$$K_{(N)LO),M_Q}^{QCD} = \frac{V_{FIN,M_Q}^{((N)LO)}}{V_{FIN,HEFT}^{((N)LO)}}, \quad (13)$$

where the subscript M_Q denotes the QCD background of a heavy quark of mass M_Q, $y_Q = M_Q/v$, and V_{FIN} as defined in the Appendix. The two-loop virtual QCD amplitude is renormalized in a five-flavor decoupling scheme. We account for heavy quark-mass effects in the QCD amplitudes by rescaling with $K_{(N)LO),M_Q}^{QCD}$, listed in Table II, and we assign an uncertainty of $\pm 50\%$ of the estimated NLO effect based on the unknown (hard) real-emission contributions.

(2) *Top quark effects* in the LO EW amplitudes were studied in Refs. [44,45] and amount to -1.8% of the LO cross section. We assign an uncertainty of the

TABLE II. K factors defined as in Eq. (13) for different heavy quark masses $M_Q = M_c, M_b, M_t$.

Quark	M_Q [GeV]	$K_{\text{LO},M_Q}^{\text{QCD}}$	$K_{\text{NLO},M_Q}^{\text{QCD}}$
Charm	1.3	−0.010	−0.018
Bottom	4.2	−0.042	−0.069
Top	173	1.032	1.031

same size based on the unknown top quark contribution in the NLO EW amplitudes.

(3) *Higher-order QCD corrections* can be accounted for under the assumption that the EW form factor receives the same QCD correction as the HEFT operator:

$$\sigma_{gg\to H+X}^{(\alpha_s^4+\alpha_s^5)\alpha^2} = \sigma_{gg\to H+X}^{(\alpha_s^2+\alpha_s^3)\alpha^2} \frac{\sigma_{gg\to H+X}^{(\alpha_s^4+\alpha_s^5)\alpha}}{\sigma_{gg\to H+X}^{(\alpha_s^2+\alpha_s^3)\alpha}}, \qquad (14)$$

and we assign an uncertainty Δ_{fact} as

$$\Delta_{\text{fact}} = \pm\delta_{\text{fact}}\sigma_{gg\to H+X}^{(\alpha_s^4+\alpha_s^5)\alpha^2} \qquad (15)$$

with

$$\delta_{\text{fact}} = \left| \frac{\frac{\sigma_{gg\to H+X}^{(\alpha_s^2\alpha^2)}}{\sigma_{gg\to H+X}^{(\text{HEFT},\alpha_s^3\alpha)}}\sigma_{gg\to H+X}^{(\text{HEFT},\alpha_s^3\alpha)}}{\sigma_{gg\to H+X}^{(\alpha_s^3\alpha^2)}} - 1 \right|$$

$$= \begin{cases} 0.15; & \mu_{R/F} = M_H \\ 0.17; & \mu_{R/F} = \frac{M_H}{2} \end{cases}, \qquad (16)$$

based on testing this EW-QCD factorization hypothesis on our exact NLO correction. We compute the higher orders in QCD with the program iHixs 2 [82]. When combining the additional contributions and uncertainties above in the setup of Table I, we arrive at our best estimate for the EW contribution of gluon-initiated Higgs production:

$$\sigma_{gg\to H+X}^{(\text{EW,best})} = \sigma_{gg\to H+X}^{(\text{HEFT},\alpha_s^2\alpha+\alpha_s^3\alpha)} \times (4.81\% \quad \text{(our computation)}$$

$$+ 0.15 \pm 0.04\% \text{ (top mass effects in QCD amp)}$$

$$- 0.27 \pm 0.09\% \text{ (bottom quark effects in QCD amp)}$$

$$- 0.07 \pm 0.02\% \text{ (charm quark effects in QCD amp)}$$

$$- 0.04 \pm 0.04\% \text{ (top quark effects in EW)}$$

$$+ 2.5 \pm 0.4\% \text{ (QCD higher orders))}$$

$$= \sigma_{gg\to H+X}^{(\text{HEFT},\alpha_s^2\alpha+\alpha_s^3\alpha)} \times (7.11 \pm 0.6\%) \qquad (17)$$

$$= 2.17 \pm 0.18 \text{ pb.} \qquad (18)$$

A similar computation for $\mu_{R/F} = \frac{1}{2}M_H$ yields $\sigma_{gg\to H+X}^{(\text{EW,best})} = 2.02 \pm 0.14$ pb.

Quark-induced and other EW contributions: The PDF suppression from qq production channels renders them negligible, and we only consider here qg-induced channels. We identify the following two categories of quark-induced contributions:

(1) *One-loop EW contributions* start at $\mathcal{O}(\alpha_s^2\alpha^2)$ for the process $qg \to Hq$ and involve one-loop EW triangle and box diagrams interfering with the one-loop QCD Higgs amplitude with exact top and bottom quark mass dependence. They can be computed exactly using the loop-induced module [83] of MG5aMC together with the loop-ready EW UFO model of Ref. [84]. We, however, use here the result of Table 3 of Ref. [47], which includes *all* one-loop EW contributions in the gg and qg channels (including Higgs-strahlung), and we refer to them for drawings of the relevant diagram classes. We assign a theoretical uncertainty to this contribution based on the 38% μ_R scale variation of its qg component of order $\mathcal{O}(\alpha_s^2\alpha^2)$, and we obtain

$$\sigma_{\text{1-loop}}^{(\text{EW})} = \begin{cases} 0.025 \pm 0.052 \text{ pb}; & \mu_{R/F} = M_H \\ 0.031 \pm 0.062 \text{ pb}; & \mu_{R/F} = \frac{M_H}{2} \end{cases}.$$

The large uncertainty assigned here reflects the accidental cancellation found among all contributions considered in Ref. [47].

(2) *Quark corrections to EW form factors* correspond to qg contributions stemming from the QCD evolution of the initial-state gluon entering the EW two-loop form factor as shown in Fig. 6. We estimate this contribution by rescaling our LO mixed QCD-EW result by the qg K factor of the HEFT contribution. This rescaling does not capture the nonuniversal unknown (hard) real emission contribution, and we assign 30% uncertainty based on these effects at NLO. However, the factorization-scale dependence of the qg channel will be captured well, since it effectively amounts to replacing the reduced matrix element, as indicated in Fig. 6. After combining both qg and gg channels, the factorization-scale dependence is reduced, and we assign an uncertainty of 10% based on the relative difference of the μ_F dependence of the NLO EW and NLO HEFT gluon-induced contributions. To estimate the higher-order QCD corrections, we perform the same rescaling and assign an uncertainty of 50% based on the fact that we do not know if they are captured well by a factorization ansatz. We obtain

$$\sigma_{qg\to H+X}^{(\text{EW})} = \begin{cases} -0.10 \pm 0.05 \text{ pb}; & \mu_{R/F} = M_H \\ 0.12 \pm 0.05 \text{ pb}; & \mu_{R/F} = \frac{M_H}{2} \end{cases},$$
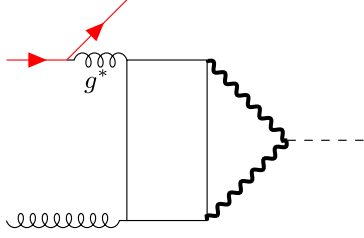
FIG. 6.   Representative diagram of the qg-initiated contribution to the NLO mixed EW-QCD cross section. Curly lines denote gluons, wavy lines correspond to massive weak gauge bosons, continuous straight lines denote massless quarks, and the dashed line represents the Higgs boson.

where we used the program iHixs 2 to compute the QCD corrections beyond NLO. Notice that, as expected, including $\sigma^{(\mathrm{EW})}_{qg \to H+X}$ helps to reduce the difference in the quantity $\sigma^{(\mathrm{EW,best})}_{gg \to H+X}$ when computed with $\mu_F = M_H$ and $\mu_F = \frac{M_H}{2}$.

(3) *Higher-order EW contributions* are estimated by reweighting our cross section with

$$K^{\text{pure-EW}}_{(\mathrm{N})\mathrm{LO}} = \frac{V^{((\mathrm{N})\mathrm{LO})}_{\mathrm{FIN,pure\text{-}EW}}}{V^{((\mathrm{N})\mathrm{LO})}_{\mathrm{FIN,mixed\text{-}QCD\text{-}EW}}}, \qquad (19)$$

where we compute $V^{((\mathrm{N})\mathrm{LO})}_{\mathrm{FIN},EW}$ by squaring (interfering) the relevant two- and three-loop EW virtual amplitudes and assign a 50% uncertainty on the NLO result based on the unknown (hard) real radiation:

$$\sigma^{(\text{squared EW})}_{gg \to H+X} = \begin{cases} 0.018 \pm 0.005 \text{ pb}; & \mu_{R/F} = M_H \\ 0.020 \pm 0.005 \text{ pb}; & \mu_{R/F} = \frac{M_H}{2} \end{cases}.$$

Together with the gluon-induced contributions of Eq. (18), we finally construct our best estimate for the overall contributions of EW origin to Higgs hadroproduction with the parameters given in Table I:

$$\sigma^{(\mathrm{EW,best})}_{pp \to H+X}$$

$$= \begin{cases} (6.91 \pm 0.9\%) \times \sigma^{(\mathrm{HEFT},\alpha_s^2\alpha + \alpha_s^3\alpha)}_{gg \to H+X}; & \mu_{R/F} = M_H \\ (6.43 \pm 0.8\%) \times \sigma^{(\mathrm{HEFT},\alpha_s^2\alpha + \alpha_s^3\alpha)}_{gg \to H+X}; & \mu_{R/F} = \frac{M_H}{2} \end{cases}$$

$$= \begin{cases} 2.11 \pm 0.28 \text{ (theory) pb}; & \mu_{R/F} = M_H \\ 2.19 \pm 0.26 \text{ (theory) pb}; & \mu_{R/F} = \frac{M_H}{2} \end{cases}. \qquad (20)$$

IV. CONCLUSION

We evaluated the NLO QCD correction to the mixed EW-QCD light-quark contribution to Higgs production via gluon fusion. Unlike previous computations of this quantity, we retained the exact dependence on the weak boson masses. The two-loop real-emission amplitudes were computed by solving differential equations for the relevant scalar integrals at runtime in terms of one-dimensional generalized power series. We implemented the resulting matrix elements in a flexible manner by encoding them as form factors of a UFO model, which we made publicly available as a MadGraph5_aMC@NLO plugin. We performed the phase-space integration numerically in two separate implementations of the FKS and COLORFUL subtraction scheme using an offline parallelization model in order to accommodate the evaluation speed of our matrix elements.

We presented the distribution of the Higgs rapidity, which shows a flat differential K-factor, and of the Higgs transverse momentum, whose spectrum is softer than its HEFT counterpart when ignoring quark mass effects.

When related to the NLO-accurate HEFT cross section, we find the EW contribution from light quarks to be 5.1% for $\mu_R = \mu_F = \frac{1}{2}M_H$, which is very close to the result of 5.2% obtained in the infinite weak boson mass limit [20,24,50]. Our result therefore allows us to reduce the uncertainty of $\pm 1\%$ assigned thus far to the mixed QCD-EW contribution in order to reflect the absence of an exact weak boson mass treatment at NLO. We also conclude that violations to the factorization of EW and QCD contributions are modest. This gives further confidence in the rescaling of our cross section with higher-order QCD corrections computed in HEFT which, together with the estimate of other partially unknown effects, yields our best estimate of $6.91 \pm 0.93\%$ (relative to the gluon-induced NLO HEFT) for the overall contribution of EW origin to Higgs production at the LHC. The LO and NLO quark-induced EW contributions now stand as an important remaining source of uncertainty, and they can be computed in the future using the same methods as those presented in this work.

ACKNOWLEDGMENTS

APPENDIX: BENCHMARK NUMERICAL MATRIX ELEMENT EVALUATIONS

In order to facilitate the reproduction of our work, we report here benchmark numerical results of our matrix

elements, summed/averaged over helicity and color configurations, evaluated for specific kinematic configurations with $\alpha_S(M_Z) = 0.118$ and all other SM parameters as in Table I. For the virtual matrix element, we only report the finite part as defined in Eq. (B.2) of Ref. [73] or Eq. (A.1) of Ref. [85]. The $gg \to H$ matrix elements are

$$V_{\text{FIN}}^{(\text{LO})} = \overline{\sum_{h,c}} 2\Re[\mathcal{A}_{gg \to H}^{(2\text{-loop})} \mathcal{A}_{\text{HEFT}}^{(\text{tree})\star}]$$

$$= 5.1508192663885 \times 10^{-4} \; [\text{GeV}^2], \quad (\text{A1})$$

$$V_{\text{FIN}}^{(\text{NLO})} = \overline{\sum_{h,c}} 2\Re[\mathcal{A}_{gg \to H}^{(3\text{-loop})} \mathcal{A}_{\text{HEFT}}^{(\text{tree})\star} + \mathcal{A}_{gg \to H}^{(2\text{-loop})} \mathcal{A}_{\text{HEFT}}^{(1\text{-loop})\star}]_{\text{FIN}}$$

$$= 3.6824078313996 \times 10^{-4} \; [\text{GeV}^2]. \quad (\text{A2})$$

We also provide the relation of $V_{\text{FIN}}^{(\text{NLO})}$ above with the matrix element M_{FIN, I_1} obtained from the finite amplitudes computed with the methods of Refs. [48,72]:

$$V_{\text{FIN}}^{(\text{NLO})} = M_{\text{FIN}, I_1} + C_A \pi^2 V_{\text{FIN}}^{(\text{LO})}, \quad (\text{A3})$$

where $C_A = 3$ denotes the number of colors. Finally, we give the two-loop $gg \to Hg$ matrix elements evaluated at two different benchmark kinematic points specified with the two Mandelstam invariants $s = (p_{g_1} + p_{g_2})^2$ and $t = (p_{g_2} - p_H)^2$:

$$\overline{\sum_{h,c}} 2\Re[\mathcal{A}_{gg \to Hg}^{(2\text{-loop})} \mathcal{A}_{\text{HEFT}}^{(\text{tree})\star}](s = 5M_H^2, t = -3M_H^2)$$

$$= 9.0303320385123 \times 10^{-6} \; [\text{GeV}^0], \quad (\text{A4})$$

$$\overline{\sum_{h,c}} 2\Re[\mathcal{A}_{gg \to Hg}^{(2\text{-loop})} \mathcal{A}_{\text{HEFT}}^{(\text{tree})\star}](s = 5M_H^2, t = -2M_H^2)$$

$$= 5.8988801633472 \times 10^{-6} \; [\text{GeV}^0]. \quad (\text{A5})$$

[1] G. Aad *et al.* (ATLAS Collaboration), Phys. Lett. B **716**, 1 (2012).

[2] S. Chatrchyan *et al.* (CMS Collaboration), Phys. Lett. B **716**, 30 (2012).

[3] R. V. Harlander and T. Neumann, Phys. Rev. D **88**, 074015 (2013).

[4] A. Banfi, A. Martin, and V. Sanz, J. High Energy Phys. 08 (2014) 053.

[5] A. Azatov and A. Paul, J. High Energy Phys. 01 (2014) 014.

[6] C. Grojean, E. Salvioni, M. Schlaffer, and A. Weiler, J. High Energy Phys. 05 (2014) 022.

[7] M. Schlaffer, M. Spannowsky, M. Takeuchi, A. Weiler, and C. Wymant, Eur. Phys. J. C **74**, 3120 (2014).

[8] M. Buschmann, C. Englert, D. Goncalves, T. Plehn, and M. Spannowsky, Phys. Rev. D **90**, 013010 (2014).

[9] S. Dawson, I. M. Lewis, and M. Zeng, Phys. Rev. D **90**, 093007 (2014).

[10] M. Buschmann, D. Goncalves, S. Kuttimalai, M. Schonherr, F. Krauss, and T. Plehn, J. High Energy Phys. 02 (2015) 038.

[11] D. Ghosh and M. Wiebusch, Phys. Rev. D **91**, 031701 (2015).

[12] S. Dawson, I. M. Lewis, and M. Zeng, Phys. Rev. D **91**, 074012 (2015).

[13] U. Langenegger, M. Spira, and I. Strebel, arXiv:1507.01373.

[14] A. Azatov, C. Grojean, A. Paul, and E. Salvioni, J. High Energy Phys. 09 (2016) 123.

[15] M. Grazzini, A. Ilnicka, M. Spira, and M. Wiesemann, J. High Energy Phys. 03 (2017) 115.

[16] H. Georgi, S. Glashow, M. Machacek, and D. V. Nanopoulos, Phys. Rev. Lett. **40**, 692 (1978).

[17] D. Graudenz, M. Spira, and P. M. Zerwas, Phys. Rev. Lett. **70**, 1372 (1993).

[18] M. Spira, A. Djouadi, D. Graudenz, and P. M. Zerwas, Nucl. Phys. **B453**, 17 (1995).

[19] R. V. Harlander and W. B. Kilgore, Phys. Rev. Lett. **88**, 201801 (2002).

[20] C. Anastasiou and K. Melnikov, Nucl. Phys. **B646**, 220 (2002).

[21] V. Ravindran, J. Smith, and W. L. van Neerven, Nucl. Phys. **B665**, 325 (2003).

[22] C. Anastasiou, C. Duhr, F. Dulat, F. Herzog, and B. Mistlberger, Phys. Rev. Lett. **114**, 212001 (2015).

[23] B. Mistlberger, J. High Energy Phys. 05 (2018) 028.

[24] C. Anastasiou, C. Duhr, F. Dulat, E. Furlan, T. Gehrmann, F. Herzog, A. Lazopoulos, and B. Mistlberger, J. High Energy Phys. 05 (2016) 058.

[25] R. Harlander and P. Kant, J. High Energy Phys. 12 (2005) 015.

[26] C. Anastasiou, S. Beerli, S. Bucherer, A. Daleo, and Z. Kunszt, J. High Energy Phys. 01 (2007) 082.

[27] U. Aglietti, R. Bonciani, G. Degrassi, and A. Vicini, J. High Energy Phys. 01 (2007) 021.

[28] R. Bonciani, G. Degrassi, and A. Vicini, J. High Energy Phys. 11 (2007) 095.

[29] C. Anastasiou, S. Bucherer, and Z. Kunszt, J. High Energy Phys. 10 (2009) 068.

[30] C. Anastasiou, N. Deutschmann, and A. Schweitzer, J. High Energy Phys. 07 (2020) 113.

[31] R. V. Harlander, M. Prausa, and J. Usovitsch, J. High Energy Phys. 10 (2019) 148.

[32] M. L. Czakon and M. Niggetiedt, J. High Energy Phys. 05 (2020) 149.

[33] M. Prausa and J. Usovitsch, arXiv:2008.11641.

[34] R. Bonciani, V. Del Duca, H. Frellesvig, J. M. Henn, F. Moriello, and V. A. Smirnov, J. High Energy Phys. 12 (2016) 096.

[35] R. Bonciani, V. Del Duca, H. Frellesvig, J. Henn, M. Hidding, L. Maestri, F. Moriello, G. Salvatori, and V. Smirnov, J. High Energy Phys. 01 (2020) 132.

[36] H. Frellesvig, M. Hidding, L. Maestri, F. Moriello, and G. Salvatori, J. High Energy Phys. 06 (2020) 093.

[37] V. Del Duca, W. Kilgore, C. Oleari, C. Schmidt, and D. Zeppenfeld, Nucl. Phys. **B616,** 367 (2001).

[38] L. Budge, J. M. Campbell, G. De Laurentis, R. K. Ellis, and S. Seth, J. High Energy Phys. 05 (2020) 079.

[39] R. V. Harlander and K. J. Ozeren, J. High Energy Phys. 11 (2009) 088.

[40] A. Pak, M. Rogal, and M. Steinhauser, J. High Energy Phys. 02 (2010) 025.

[41] R. V. Harlander, T. Neumann, K. J. Ozeren, and M. Wiesemann, J. High Energy Phys. 08 (2012) 139.

[42] U. Aglietti, R. Bonciani, G. Degrassi, and A. Vicini, Phys. Lett. B **595,** 432 (2004).

[43] U. Aglietti, R. Bonciani, G. Degrassi, and A. Vicini, Phys. Lett. B **600,** 57 (2004).

[44] G. Degrassi and F. Maltoni, Phys. Lett. B **600,** 255 (2004).

[45] S. Actis, G. Passarino, C. Sturm, and S. Uccirati, Phys. Lett. B **670,** 12 (2008).

[46] C. Anastasiou, R. Boughezal, and F. Petriello, J. High Energy Phys. 04 (2009) 003.

[47] V. Hirschi, S. Lionetti, and A. Schweitzer, J. High Energy Phys. 05 (2019) 002.

[48] M. Bonetti, K. Melnikov, and L. Tancredi, Nucl. Phys. **B916,** 709 (2017).

[49] M. Bonetti, K. Melnikov, and L. Tancredi, Phys. Rev. D **97,** 056017 (2018); **97,** 099906(E) (2018).

[50] C. Anastasiou, V. del Duca, E. Furlan, B. Mistlberger, F. Moriello, A. Schweitzer, and C. Specchia, J. High Energy Phys. 03 (2019) 162.

[51] M. Becchetti, R. Bonciani, V. Casconi, V. Del Duca, and F. Moriello, J. High Energy Phys. 12 (2018) 019.

[52] M. Bonetti, E. Panzer, V. A. Smirnov, and L. Tancredi, J. High Energy Phys. 11 (2020) 045.

[53] F. Moriello, J. High Energy Phys. 01 (2020) 150.

[54] P. Maierhoefer, J. Usovitsch, and P. Uwer, Comput. Phys. Commun. **230,** 99 (2018).

[55] A. V. Smirnov, Comput. Phys. Commun. **189,** 182 (2015).

[56] R. N. Lee, J. Phys. Conf. Ser. **523,** 012059 (2014).

[57] K. Chetyrkin and F. Tkachov, Nucl. Phys. **B192,** 159 (1981).

[58] F. Tkachov, Phys. Lett. **100B,** 65 (1981).

[59] S. Laporta, Int. J. Mod. Phys. A **15,** 5087 (2000).

[60] T. Gehrmann and E. Remiddi, Nucl. Phys. **B580,** 485 (2000).

[61] A. Kotikov, Phys. Lett. B **254,** 158 (1991).

[62] E. Remiddi, Nuovo Cimento A **110,** 1435 (1997).

[63] T. Gehrmann and E. Remiddi, Nucl. Phys. **B640,** 379 (2002).

[64] M. Argeri and P. Mastrolia, Int. J. Mod. Phys. A **22,** 4375 (2007).

[65] J. M. Henn, Phys. Rev. Lett. **110,** 251601 (2013).

[66] J. M. Henn, J. Phys. A **48,** 153001 (2015).

[67] M. Argeri, S. Di Vita, P. Mastrolia, E. Mirabella, J. Schlenk, U. Schubert, and L. Tancredi, J. High Energy Phys. 03 (2014) 082.

[68] R. N. Lee, J. High Energy Phys. 04 (2015) 108.

[69] A. Georgoudis, K. J. Larsen, and Y. Zhang, Comput. Phys. Commun. **221,** 203 (2017).

[70] T. Gehrmann, A. von Manteuffel, L. Tancredi, and E. Weihs, J. High Energy Phys. 06 (2014) 032.

[71] M. Becchetti and R. Bonciani, J. High Energy Phys. 01 (2018) 048.

[72] M. Bonetti, K. Melnikov, and L. Tancredi, Phys. Rev. D **97,** 034004 (2018).

[73] R. Frederix, S. Frixione, F. Maltoni, and T. Stelzer, J. High Energy Phys. 10 (2009) 003.

[74] S. Lionetti, Ph.D. thesis, ETH, 2018.

[75] V. Del Duca, N. Deutschmann, and S. Lionetti, J. High Energy Phys. 12 (2019) 129.

[76] G. Somogyi and Z. Trocsanyi, arXiv:hep-ph/0609041.

[77] G. Somogyi, J. High Energy Phys. 05 (2009) 016.

[78] C. Degrande, C. Duhr, B. Fuks, D. Grellscheid, O. Mattelaer, and T. Reiter, Comput. Phys. Commun. **183,** 1201 (2012).

[79] J. Alwall, R. Frederix, S. Frixione, V. Hirschi, F. Maltoni, O. Mattelaer, H. S. Shao, T. Stelzer, P. Torrielli, and M. Zaro, J. High Energy Phys. 07 (2014) 079.

[80] M. Whalley, D. Bourilkov, and R. Group, in *HERA and the LHC: A Workshop on the Implications of HERA and LHC Physics* (Startup Meeting, CERN, 2004; Midterm Meeting, CERN, 2004) (2005), pp. 575–581.

[81] K. Becker *et al.*, arXiv:2005.07762.

[82] F. Dulat, A. Lazopoulos, and B. Mistlberger, Comput. Phys. Commun. **233,** 243 (2018).

[83] V. Hirschi and O. Mattelaer, J. High Energy Phys. 10 (2015) 146.

[84] R. Frederix, S. Frixione, V. Hirschi, D. Pagani, H.-S. Shao, and M. Zaro, J. High Energy Phys. 07 (2018) 185.

[85] V. Hirschi, R. Frederix, S. Frixione, M. V. Garzelli, F. Maltoni, and R. Pittau, J. High Energy Phys. 05 (2011) 044.